Use of Secondary Reinforcement to Minimize Lateral Deformation of Geosynthetic-Reinforced Retaining Walls: Numerical Analysis

Yan Jiang[1]; Jie Han[2]; Robert L. Parsons[3]

[1] Terracon Consultants, Inc., 2201 Rowland Ave, Savannah, Georgia 31404, USA. Email: yan.jiang@terracon.com (corresponding author)

[2] Department of Civil, Environmental, & Architectural Engineering, the University of Kansas, USA. Email: jiehan@ku.edu

[3]Department of Civil, Environmental, & Architectural Engineering, the University of Kansas, USA. Email: rparsons@ku.edu

Abstract:

Field monitoring has demonstrated that secondary reinforcement could reduce the maximum deformation of geosynthetic-reinforced retaining (GRR) walls. However, the effect of secondary reinforcement on the reduction of lateral deformations of GRR walls has not been well studied yet. This study used a finite difference method incorporated in the Fast Lagrangian Analysis of Continua (FLAC) software to develop two-dimensional (2D) numerical models and assess the effect of secondary reinforcement on the reduction of lateral deformations of GRR walls. These models used an advanced soil constitutive model based on the theory of hardening plasticity, called the Cap-Yield (CY) model, to simulate the behavior of backfill. The numerical model was first calibrated and verified against the measured results from a full-scale field test. A parametric study was conducted to investigate the effects of four factors related to secondary reinforcement including secondary reinforcement length, secondary reinforcement stiffness, secondary reinforcement connection, and secondary reinforcement layout. The numerical results show an increase in secondary reinforcement length and stiffness can reduce the lateral deformations of GRR walls. The mechanical connection of secondary reinforcement can also reduce the wall facing deflection. In addition, the wall with a special layout (i.e., fewer but longer secondary reinforcement layers at certain elevations) had relatively smaller wall facing deflections. The results of this study will reduce the lateral deformation of GRR walls with less use of geosynthetics and benefit the geosynthetics community by providing an economical and practical solution for high GRE walls. Also, an equation to estimate the lateral deformation of GRR walls with secondary reinforcement was proposed. The factors that affect the reduction factor (F) were also discussed.

1. Introduction

Field monitoring has demonstrated that secondary reinforcement could reduce the maximum deformation of geosynthetic-reinforced retaining (GRR) walls. Jiang et al. (2015 and 2016) found that the secondary reinforcement not only could reduce the connection forces and maximum tensile stresses in geogrids, but also could reduce wall deflections. Although field testing is a straightforward and effective method for studying the effect of the secondary reinforcement on the behavior of GRR walls, it is costly and time-consuming as compared with numerical modeling.

Many researchers have successfully used the numerical modeling to study the behavior of GRR walls (e.g., Christopher et al. 1989; Ho and Rowe 1996; Leshchinsky and Vulova 2001; Ling and Leshchinsky 2003; Hatami and Bathurst 2006; Guler et al. 2007; Huang et al. 2013; Yu et al. 2017; Gu et al. 2017; Han et al. 2018; Shen et al. 2019; Jiang et al. 2019). Leshchinsky and Vulova (2001) used the numerical modeling to investigate the influence of secondary reinforcement on failure modes of GRR walls. Their study illustrated that the inclusion of secondary reinforcement could reduce the connection load in the primary reinforcement, increase internal wall stability, and change the failure mode from reinforcement connection failure to compound failure. Jiang et al. (2019) also used the numerical modeling to evaluate the performance of a well-instrumented GRR wall with secondary reinforcement. Their numerical results demonstrate that the secondary reinforcement cannot only reduce the connection forces and maximum tensile stresses in geogrids but also reduce wall deflection. Although few studies have demonstrated that the use of secondary reinforcement is able to minimize wall deflection. However, the effect of secondary reinforcement on the reduction of lateral deformations of GRR walls has not been well studied yet.

In this study, a two-dimensional (2D) finite differential software program, FLAC2D, was employed to develop numerical models to evaluate the effect of the secondary reinforcement on the performance of the GRR walls. The Cap-Yield (CY) model, a nonlinear elastic-plastic soil constitutive model as used by Huang et al. (2013), was employed to simulate the behavior of backfill. All geosynthetic reinforcement materials including primary and secondary reinforcement layers were modeled as a linearly elastic-perfectly plastic material. All the numerical models also included a block-block interface, block-backfill interface, backfill-geosynthetic reinforcement interface, compaction induced stress, and construction procedure of GRR walls with secondary reinforcement. The numerical model was first calibrated and verified using the measured results from full-scale field testing. A parametric study was performed to evaluate the effects of secondary

reinforcement length, secondary reinforcement stiffness, secondary reinforcement connection, and secondary reinforcement layout, on the performance of the GRR wall.

2. Baseline Model

2.1 Numerical Model Dimensions

A 2D numerical model used in this study was created and modified from a numerical model that was developed to analyze an instrumented wall (Jiang et al. 2019). The developed numerical model was verified by the measured results from a full-scale field test and the details of the numerical model verification could be found in Jiang et al (2019). Fig. 1 shows the mesh of the numerical model used in this study. The entire numerical model consisted of a foundation, an embedment soil, wall facing, a reinforced soil zone, and a retained soil zone. The primary reinforcement length (L_p) was 0.7 times the wall height (H).

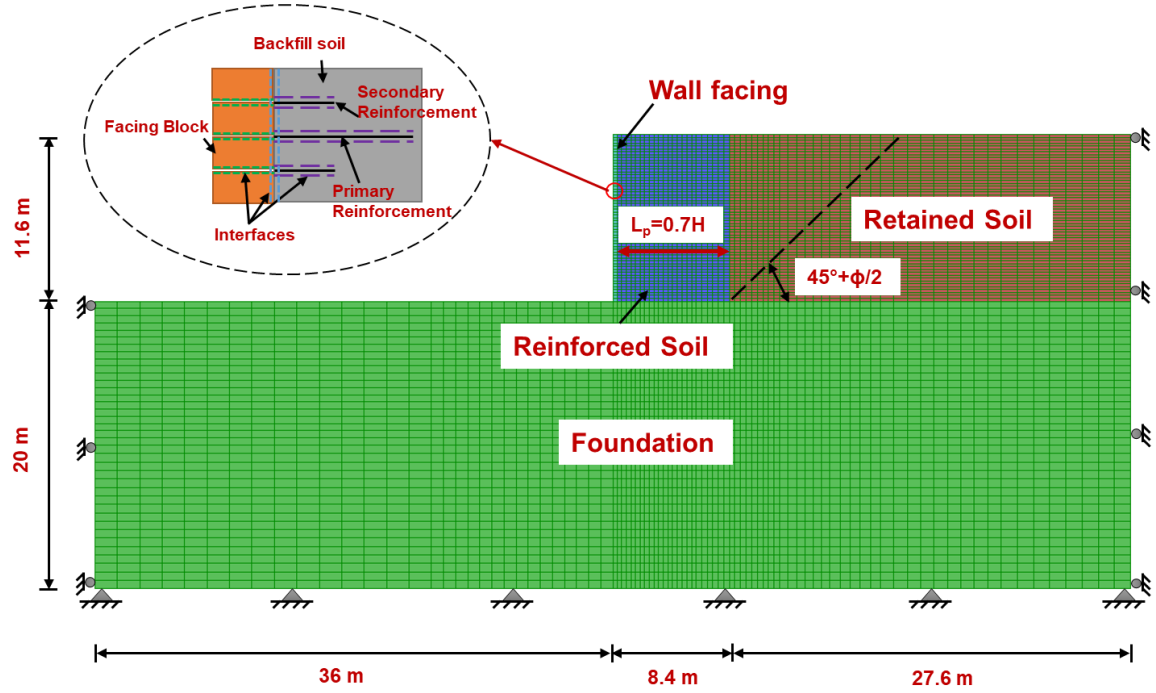

Fig. 1. Mesh of the baseline model

Fig. 1 shows that the foundation soil in the numerical model was 20 m deep and 72 m wide. The height of the wall facing in the numerical model was 11.6 m including 58 stacked facing blocks. The height and nominal width of the facing blocks were 0.2 and 0.3 m, respectively. The primary reinforcement length was 8.1 m, which were equal to 70% of the wall height. The secondary reinforcement length was 1.5 m in the baseline case. The vertical spacing of the primary reinforcement was 0.6 m. The secondary reinforcement layers were installed at vertical spacing of 0.2 m between two primary reinforcement layers as shown in Fig. 1. To minimize boundary effects, the width of the retained soil zone was extended to 27.6 m. Fig. 1 also shows the boundary conditions used in the numerical model. The vertical and horizontal displacements at the bottom of the model were set to zero. The horizontal displacements at the left and right sides were set to zero while the vertical displacements at the left and right sides were set to be free.

2.2 Constitutive Models and Properties

The behavior backfill in the baseline model was simulated using the Cap-Yield (CY) model. Other soil constitutive models (e.g., the Mohr-Coulomb model and the nonlinear hyperbolic model proposed by Duncan et al. 1980) have been used in the simulation of GRR walls by other researchers (Hatami and Bathurst 2006 and Yu et al. 2018). However, the CY model has its advantages and features: (1) to model the hardening behavior of volumetric strain under isotropic compression; (2) to simulate soil modulus decrease and plastic deformation subjected to shear loading; and (3) to exhibit dilative characteristics. The detailed description and theoretical background of the CY model can be found in Itasca (2011). The parameters of the CY model for the backfill are listed in Table 1, which have been determined, calibrated, and verified by Jiang et al. (2019).

Table 1. Parameters of the Cap-Yield model for the backfill

Parameters	γ (kN/m^3)	α	ϕ (°)	ψ (°)	R	β	G^e_{ref} (kPa)	K^{iso}_{ref} (kPa)	P_{ref} (kPa)	ν_{ur}	c (kPa)	m	R_f
Value	18.1	1.5	52	8	6.2	0.5	32500	6971	100	0.2	0	0.52	0.9

Note: γ= unit weight; α= Cap-Yield surface parameter; ϕ = friction angle; ψ = dilation angle; R=multiplier; β= plastic strain coefficient; G^e_{ref} =reference elastic tangent shear modus; K^{iso}_{ref}=reference bulk modulus; P_{ref} = reference pressure; ν_{ur} = Poisson's ratio; c= cohesion; m= power; and R_f= failure ratio.

The retained soil was modeled as a linearly elastic-perfectly plastic material with the Mohr-Coulomb failure criterion. The foundation soil of the GRR walls in this paper was assumed to be firm like bedrock. The foundation soil and the block facing were modeled as a linearly elastic material with their parameters summarized in Table 2.

Table 2. Parameters of retained and foundation soils and block facing in the numerical model

Material	Constitutive model	Unit weight (kN/m^3)	Young's modulus (MPa)	Poisson's ratio	Cohesion (kPa)	Friction angle (°)	Dilation angle (°)
Retained soil	Mohr-Coulomb	16.8	20	0.3	1	34	0
Foundation soil	Linearly elastic	20.0	2000	0.2	0	0	0
Block facing	Linearly elastic	15.0	2000	0.25	-	-	-

A strip element was selected to simulate the behavior of geogrid reinforcement. The strip element was developed in FLAC to model geogrid or steel reinforcement in earth retaining structures. The reinforcement in this study was modeled as a linearly elastic-perfectly plastic material. Table 3 summarizes the parameters of reinforcement in the numerical simulation.

Table 3. Parameters of geogrid reinforcement in the numerical model

Materials	Structure element type	Constitutive model	Secant stiffness (kN/m)	Yield strength (kN/m)	Tensile failure strain (%)
Primary reinforcement	Strip	Linearly elastic-perfectly plastic	1000	114	10
Secondary reinforcement			500	58	10

Note: * stiffness in the cross-machine direction

2.3 Interface Properties

Three types of interfaces were used in the numerical model: (1) backfill-reinforcement interface; (2) block-block interface; and (3) block-backfill interface. All these interfaces were modeled as linearly elastic-perfectly plastic materials with the Mohr-Coulomb failure criterion. This interface model has been successfully used in the numerical simulation of GRR walls by other researchers, such as Yu et al. (2017). A detailed discussion on the interfaces can be found in Jiang et al. (2019). Table 4 lists the parameters of the interfaces.

Table 4. Interface parameters

Interface	Friction angle (°)	Dilation angle (°)	Cohesion (kPa)	Normal stiffness, k_n (MN/m/m)	Shear stiffness, k_s (MN/m/m)
Backfill-reinforcement	40	0	0	-	6.5
Block-block	57	0	46	1000	40
Block-backfill	40	8	0	100	1

2.4 Construction Procedure

The numerical model simulated the construction of the wall. A detailed description of the simulated construction procedure can be found in Jiang et al. (2019). All the reinforcement layers were connected to facing blocks at the same elevation through pin connections in the baseline case. The pin connections make the reinforcement layers and their connected facing blocks have the same displacement at the connection points; however, each reinforcement layer rotates freely around the pin point. This connection is often referred to as a mechanical connection.

There is no well-accepted method to simulate compaction stress as the compaction is a dynamic process and the accurate simulation of soil response under such loading process is difficult. Jiang et al. (2019) summarized the methods of the compaction stress simulation in the past numerical studies. Mirmoradi and Ehrlich (2015 and 2018) presented three types of the numerical simulation of the compaction stress. They recommended to use distributed loads applied at the top and bottom of each backfill layer to simulate the compaction stress. However, other studies (Yu et al. 2017; Jiang et al. 2019) demonstrated that the compaction stress could be approximately simulated using a distributed load applied at the top of each backfill layer. In this study, the compaction stress was modeled by applying an 8-kPa vertical distribution pressure on the top of each backfill lift.

3. Investigated Parameters

A parametric study was performed to evaluate the effects of the secondary reinforcement on the performance of the GRR wall in terms of wall facing deflections and tensile stresses in geosynthetic reinforcement. The major influence factors include the secondary reinforcement length, the secondary reinforcement stiffness, the secondary reinforcement connection, and the layout of secondary reinforcement. One parameter was deviated from the baseline case to investigate the influence of that specific factor. The details of the investigated factors are listed in Table 5.

Table 5 Influence factors used in parametric study

Key factors	Values
Secondary reinforcement length (m)	1.0, 1.5*, 2.0, 3.0, 4.0
Secondary reinforcement stiffness (kN/m)	100, 500*, 1000, 2000, 5000
Secondary reinforcement connection	pin connection*, no connection
Secondary reinforcement layout	even layout*, special layout

Note: * means the case used in the baseline model.

4. Numerical Results and Discussion

4.1 Effect of secondary reinforcement length

This section evaluates the effect of secondary reinforcement length on wall facing deflections. Five secondary reinforcement lengths (L) were considered and their lengths were normalized by the full wall height (H) as the secondary reinforcement length to full wall height ratio, L/H. The L/H ratio ranged from 0.09 to 0.34. The baseline model had an L/H ratio of 0.13. For comparison purposes, a case with an L/H ratio of 0 was also considered, in which there was no secondary reinforcement.

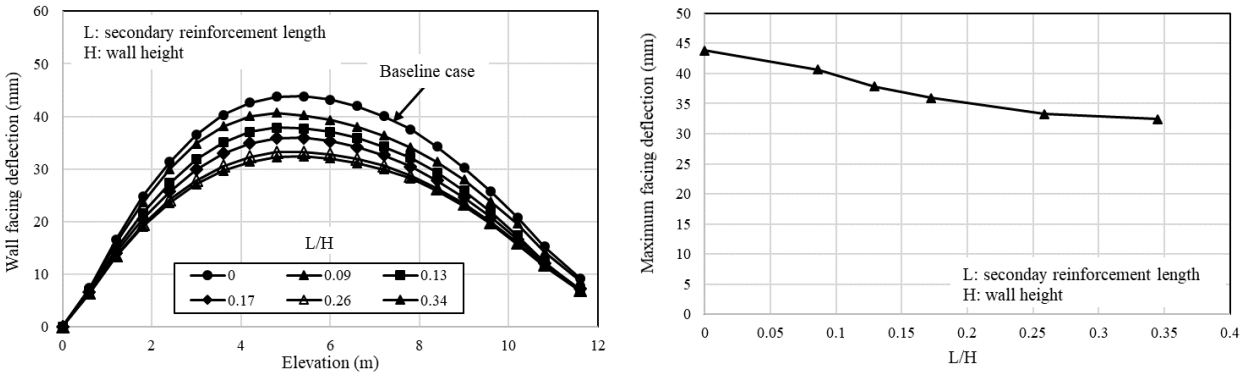

(a) (b)

Fig. 2. Effect of L/H ratios on wall facing deflection: (a) wall facing deflection profiles; (b) maximum facing deflection

Fig. 2(a) shows the profiles of the wall facing deflection along the wall elevation at different L/H ratios. The wall facing deflections were almost zero at the bottom of the walls in all the six cases. The wall facing deflection increased with the wall elevation and reached the maximum value approximately in the middle of the walls and then decreased with the elevation towards the top of the walls. The wall facing deflections decreased and converged near the top of walls in all the six cases. Also, the wall facing deflections decreased with an increase in the length of the secondary reinforcement. To show the effect of the secondary reinforcement length on the maximum wall facing deflection, a relationship between the

L/H ratio and the maximum wall facing deflection is graphed in Fig. 2(a), showing that the maximum wall facing deflection decreased rapidly with an increase in the L/H ratio when the L/H ratio was smaller than a certain value (0.26 in this study as an example). When the L/H ratio was greater than this value, the maximum wall facing deflection decreased slowly. This result indicates that the benefit of an increase in the secondary reinforcement length to minimize the maximum wall facing deflections becomes negligible when the L/H ratio is greater than the certain value. Consider two extreme conditions without and with secondary reinforcement, the maximum facing deflection reduction by secondary reinforcement is approximately 26%.

4.2 Effect of secondary reinforcement stiffness

This section evaluates the effect of the secondary reinforcement stiffness on wall facing deflections and tensile stresses in primary reinforcement. In the baseline model, the secondary reinforcement stiffness was 500 kN/m. Four additional cases with secondary reinforcement stiffness values of 100, 1000, 2000, and 5000 kN/m were studied.

Fig. 3(a) shows the profiles of the wall facing deflections with different values of secondary reinforcement stiffness, indicating that the secondary reinforcement stiffness had an influence on the profiles of the wall facing deflections along the wall elevation. The profile pattern of the wall facing deflection in Fig. 3(a) is similar to that in Fig. 2(a). In addition, the wall facing deflection decreased with an increase in the secondary reinforcement stiffness. To show the effect of the secondary reinforcement stiffness on the maximum wall facing deflection, a relationship between the secondary reinforcement stiffness and the maximum wall facing deflection is graphed in Fig. 3(b). The maximum wall facing deflection rapidly decreased with an increase in the secondary reinforcement stiffness. The secondary reinforcement stiffness had a large influence on the maximum wall facing deflection when the secondary reinforcement stiffness was lower than a certain value (2000 kN/m in this study). However, when the secondary reinforcement stiffness was higher than this value, the benefit of increasing the secondary reinforcement stiffness to reduce the maximum wall facing deflection became minimal. Consider two extreme conditions without and with stiff secondary reinforcement, the maximum facing deflection reduction by secondary reinforcement is approximately 21%.

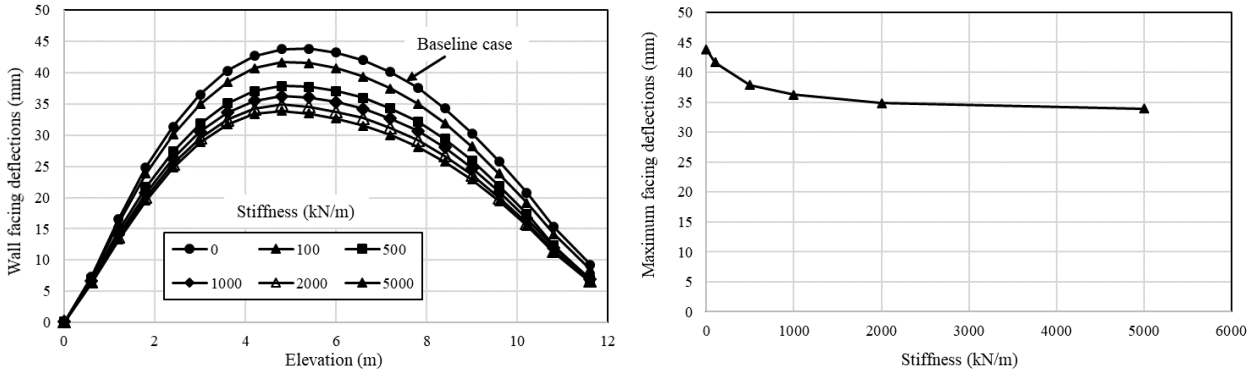

(a) (b)

Fig. 3. Effect of secondary reinforcement stiffness on wall facing deflection: (a) wall facing deflection profiles; (b) maximum facing deflection

4.3 Effect of secondary reinforcement connection

In the baseline model, the GRR wall had the secondary reinforcement connected to the modular block facing using a pin connection to simulate a mechanical connection. In some applications (e.g., geosynthetic-reinforced soil-integrated bridge system), however, secondary reinforcement may not be connected to wall facing. Therefore, the benefit of the secondary reinforcement connected to the wall facing and the performance of the GRR wall with secondary reinforcement not connected to the wall facing are worth studying. The following section examines the effect of the secondary reinforcement not connected to the wall facing on the wall facing deflections.

Fig. 4 shows the profiles of the wall facing deflections with and without secondary reinforcement connected to the wall facing. For comparison purposes, the wall without secondary reinforcement was also considered. Fig. 4 shows that the walls with and without a pin connection for secondary reinforcement had similar profile trends for the wall facing deflections. The secondary reinforcement connection had little influence on the wall facing deflection in the lower part of the wall (from the elevation of 0 to 3.0 m in this study). Above the elevation of 3.0 m, the wall connected to secondary reinforcement

had smaller wall facing deflections than the one without any connections to the secondary reinforcement. All the walls with secondary reinforcement had smaller wall facing deflections than the one without secondary reinforcement.

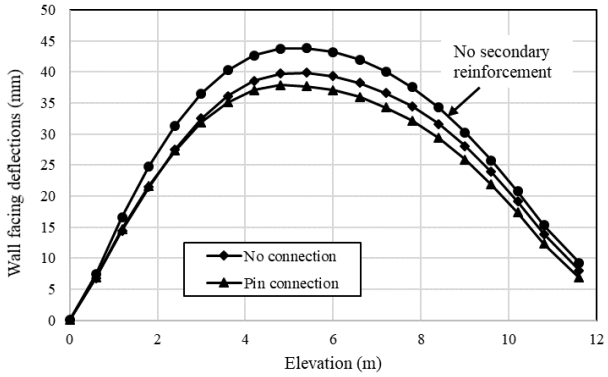

Fig. 4. Effect of secondary reinforcement connection on wall facing deflection

4.4 Effect of secondary reinforcement layout

Figs. 2 to 4 show that large wall facing deflections for the wall with secondary reinforcement mainly occurred between elevations of 2.0 and 8.0 m. Based on this finding, an increase in the secondary reinforcement length within this portion could reduce wall facing deflections. Therefore a special layout of the secondary reinforcement was investigated with the purpose of reducing wall facing deflections further while using less or a same amount of geosynthetic reinforcement material.

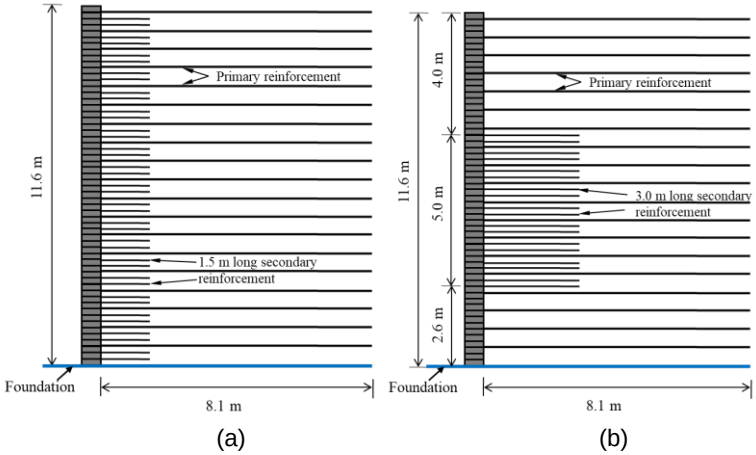

Fig. 5. Secondary reinforcement layout: (a) even layout; (b) special layout

The baseline case had the 1.5-m long secondary reinforcement layers evenly distributed between primary reinforcement along the full height of the wall (referred to as even layout in this paper). In the special layout, 3-m long secondary reinforcement layers were installed between the primary reinforcement between elevations of 2.6 and 7.6 m. The other regions did not have secondary reinforcement. In other words, the wall with the special layout had fewer reinforcement layers than that with the even layout. Fig. 5 illustrates the even and special layout of secondary reinforcement. The secondary reinforcement in the special layout had the same properties and spacing as those in the baseline case. The baseline case used a total length of secondary reinforcement of approximately 57 m (38x1.5=57 m) per meter of wall width in the longitudinal direction while the special layout used a total length of secondary reinforcement of approximately 54 m (18x3=54 m) per meter.

Fig. 6 shows the profiles of the wall facing deflections with even and special layouts of secondary reinforcement. The wall with the even and special layouts had similar wall facing deflections in the lower and upper parts of the wall. However, the wall with the special layout had relatively small wall facing deflections in the middle part of the wall as compared with the baseline case. Although the reduction in wall facing deflection is not significant, this comparison demonstrates that the special layout of the secondary reinforcement could further reduce the maximum wall facing deflections while using same or less geosynthetic reinforcement material.

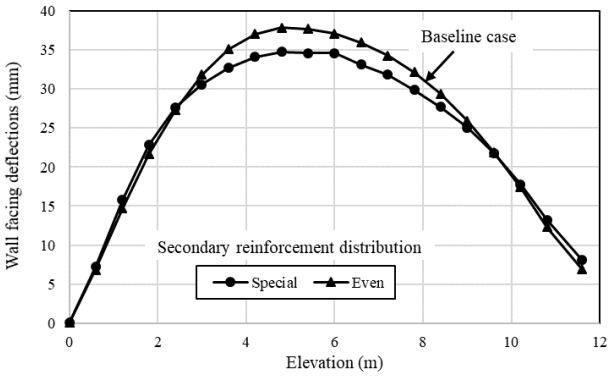

Fig. 6. Effect of secondary reinforcement layout on wall facing deflection

4.5 Estimation of lateral deformation of walls with secondary reinforcement

The numerical results show that the secondary reinforcement can reduce the lateral deformation of the wall. To estimate the lateral deformation of walls with secondary reinforcement, we proposed the following equation to consider the benefit of the secondary reinforcement to minimize the lateral deformation of the wall, which can be used in the design of GRR walls with secondary reinforcement:

$$d_{max} = F \cdot D_{max} \quad (1)$$

where d_{max} = maximum lateral deformation of walls with secondary reinforcement; D_{max} = maximum lateral deformation of walls without secondary reinforcement; F = reduction factor of lateral deformation due to secondary reinforcement.

The maximum lateral deformation of wall without secondary reinforcement (Dmax) can be obtained from measured results, numerical results, and analytical and empirical equations. Khosrojerdi et al. (2017) summarized and evaluated six analytical and empirical equations to calculate the lateral wall deformation of GRR walls and abutments. The reduction factor of lateral deformation due to secondary reinforcement (F) is closely related to the geometry, dimension, layout, and material properties of the secondary reinforcement. In this study, we understand that the F is a function of the secondary reinforcement length, secondary reinforcement stiffness, connection to wall facing, and layout in the wall. A further study is needed to investigate other factors that influence the lateral deformation of walls with secondary reinforcement. Also, to calculate the lateral deformation of walls with secondary reinforcement, a comprehensive parametric study and statistical analysis using the multiple linear regression are needed to develop an equation of the reduction factor F.

Conclusions

This study used a verified numerical model to evaluate the effects of the secondary reinforcement on lateral deformation of the GRR walls. The Cap-Yield (CY) model, a nonlinear elastic-plastic soil constitutive model, was employed to simulate the behavior of backfill. The numerical model also considered complicated interactions between different materials in the wall (e.g. a block-block interface, block-backfill interface, and backfill-geosynthetic reinforcement interface) as well as the construction procedure for GRR walls with secondary reinforcement. A parametric study was performed to investigate the effects of secondary reinforcement length, secondary reinforcement stiffness, secondary reinforcement connection, and secondary reinforcement layout on the performance of the GRR wall. The following conclusions can be drawn:

(1) The wall facing deflections decreased with an increase in the secondary reinforcement length and stiffness. The incremental benefit of increasing the secondary reinforcement length and stiffness to reduce the maximum wall facing deflections becomes negligible when the secondary reinforcement length to wall height ratio (L/H) is greater than a certain values (0.26 in this study) and the secondary reinforcement stiffness is higher than a certain value (2000 kN/m in this study), respectively.

(2) The walls with and without the pin connection for secondary reinforcement had similar wall facing deflection profiles. The pin connection for secondary reinforcement had a minimal influence on the wall facing deflection in the lower part of the wall (from the elevation of 0–3.0 m in this study). In the middle and upper parts of the wall, the wall with the pin connection for secondary reinforcement had smaller wall facing deflections than the one without any connection for secondary reinforcement.

(3) The walls with the even and special layouts had similar wall facing deflections in the lower and upper parts of the wall. However, the wall with the special layout had relatively small wall facing deflections in the middle part of the wall as compared with the baseline case. This comparison demonstrates that the special layout of the secondary reinforcement could further reduce the maximum wall facing deflections using the same or less amount of geosynthetic reinforcement material.

(4) An equation to estimate the lateral deformation of GRR walls with secondary reinforcement was proposed. The factors that affect the reduction factor (F) were also discussed. Based on the numerical results in this study, we understand that the F is a function of the secondary reinforcement length, secondary reinforcement stiffness, connection to wall facing, and layout along the wall. A further study is needed to investigate other factors that influence the lateral deformation of walls with secondary reinforcement. Also, to calculate the lateral deformation of walls with secondary reinforcement, a comprehensive parametric study and statistical analysis using the multiple linear regression are needed to obtain the function of the reduction factor F.

Acknowledgement

This study was partially sponsored by the Geosynthetic Institute through the GSI fellowship awarded to the first author.

References

Christopher, B.R., Gill, S.A., Giroud, J.P., Juran, I. Scholsser, F., Mitchell, J.K., Dunnicliff, J., 1989. Reinforced Soil Structures, Volume II. Summary of research and systems information. *Report No. FHWA-RD-89-043*, Federal Highway Administration, Washington DC, November 1989, 287p.

Duncan, J. M., Byrne, P. M., Wong, K. S., Mabry, P., 1980. Strength, stress-strain and bulk modulus parameters for finite element analyses of stresses and movements in soil masses. *Rep. No. UCB/GT/80-01*, Dept. of Civil Engineering, Univ. of California, Berkeley, CA.

Gu, M., Collin, J.G., Han, J., Zhang, Z., Tanyu, B.F., Leshchinsky, D., Ling, H. I., Rimoldi, P., 2017. Numerical analysis of instrumented mechanically stabilized gabion walls with large vertical reinforcement spacing. *Geotext. Geomembr.*, 45, 294-306,

Guler, E., Hamderi, M.,Demirkan, M. M., 2007. Numerical analysis of reinforced soil-retaining wall structures with cohesive and granular backfills. *Geosynth. Int.*, 14 (6), 330-345.

Han, J., Jiang, Y., Xu, C., 2018. Recent advances in geosynthetic-reinforced retaining walls for highway applications." *Front. Struct. Civ. Eng.* 12 (2), 239-247.

Hatami, K., Bathurst, R.J., 2006. Numerical model for reinforced soil segmental walls under surcharge loading. *J. Geotech. Geoenviron. Eng.* 132 (6), 673-684.

Ho, S.K., Rowe, R.K., 1996. Effect of wall geometry on the behaviour of reinforced soil walls. *Geotext. Geomembr.* 14 (10), 521-541.

Huang, J., Han, J., Parsons, R.L., Pierson, M.C., 2013. Refined numerical modeling of a laterally-loaded drilled shaft in an MSE wall. *Geotext. Geomembr.* 37, 61-73.

Itasca Consulting Group, 2011. FLAC: Fast Lagrangian Analysis of Continua, version 7.0, Itasca Consulting Group, Inc., Minneapolis, Minn.

Jiang, Y., Han, J., Parsons, R.L., Cai, H., 2015. Field monitoring of mse walls to investigate secondary reinforcement effects. Report No. KS-15-09, Kansas Department of Transportation.

Jiang, Y., Han, J., Parsons, R.L., Brennan, J.J., 2016. Field instrumentation and evaluation of modular-block MSE walls with secondary geogrid layers. *J. Geotech. Geoenviron. Eng.*, http://dx.doi.org/10.1061/(ASCE)GT.1943-5606.0001573, 05016002.

Jiang, Y., Han, J., Zornberg, J., Parsons, R.L., Leshchinsky, D., Tanyu, B., 2019. Numerical analysis of field geosynthetic-reinforced retaining walls with secondary reinforcement. *Geotechnique*, 69 (2), 122-132. https://doi.org/10.1680/jgeot.17.P.118.

Leshchinsky, D., Vulova, C., 2001. Numerical investigation of the effects of geosynthetic spacing on failure mechanisms of MSE block walls. *Geosynth. Int.* 8 (4), 343-365.

Ling, H.I., Leshchinsky, D., 2003. Finite element parametric study of the behavior of segmental block reinforced-soil retaining walls. *Geosynth. Int.* 10 (3), 77-94.

Mirmoradi, S.H., Ehrlich, M., 2015. Modeling of the compaction-induced stress on reinforced soil walls. *Geotext. Geomembr.* 43 (1), 82-88.

Mirmoradi, S.H., Ehrlich, M., 2018. Numerical simulation of compaction-induced stress for the analysis of GRS walls under working conditions. *Geotext. Geomembr.* 46 (3), 354-365.

Shen, P., Han, J., Zornberg, J.G., Morsy, A.M., Leshchinsky, D., Tanyu, B.F., and Xu, C., 2019. Two and three-dimensional numerical analyses of geosynthetic-reinforced soil (GRS) piers. *Geotext. Geomembr.* 47, 352-268.

Yu, Y., Bathurst, R.J., Allen, T.M., 2017. Numerical modelling of two full-scale reinforced soil wrapped-face walls. *Geotext. Geomembr.* 45 (4), 237-249.

Khosrojerdi, M., Xiao, M., Qiu, T., and Nicks, J., 2017. Evaluation of prediction methods for lateral deformation of grs walls and abutments. *J. Geotech. Geoenviron. Eng.* 143(2). https://doi.org/10.1061/(ASCE)GT.1943-5606.0001591